

Visual Simulation of Soil-Structure Destruction with Seepage Flows

XU WANG, MAKOTO FUJISAWA, and MASAHIKO MIKAWA, University of Tsukuba, Japan



Fig. 1. **Left:** Overtopping flow induces the dam breach. **Middle:** The pouring water destracts bunny soil-structure. **Right:** The flood breaks through a dam placed in the valley.

This paper introduces a method for simulating soil-structure coupling with water, which involves a series of visual effects, including wet granular materials, seepage flows, capillary action between grains, and dam breaking simulation. We develop a seepage flow based SPH-DEM framework to handle soil and water particles interactions through a momentum exchange term. In this framework, water is seen as a seepage flow through porous media by Darcy's law; the seepage rate and the soil permeability are manipulated according to drag coefficient and soil porosity. A water saturation-based capillary model is used to capture various soil behaviors such as sandy soil and clay soil. Furthermore, the capillary model can dynamically adjust liquid bridge forces induced by surface tension between soil particles. The adhesion model describes the attraction ability between soil surfaces and water particles to achieve various visual effects for soil and water. Lastly, this framework can capture the complicated dam-breaking scenarios caused by overtopping flow or internal seepage erosion that are challenging to simulate.

CCS Concepts: • Computing methodologies → Physical simulation.

Additional Key Words and Phrases: Seepage Flow, Smoothed Particle Hydrodynamics, Discrete Element Method, Capillary Action, Adhesion, Dam Breach

1 INTRODUCTION

Realistic visual simulation of natural disasters such as debris flows and landslides usually leaves people a deep impression. Over the past decades, simulations focused on interactions of multi-phase and multi-material have received much attention in computer graphics.

Previous works have developed physically-based simulation techniques using diversified particle-based, grid-based, or hybrid-based frameworks. The unified Lagrangian approach for fluid-solid interactions [Keiser et al. 2005; Solenthaler et al. 2007] relies on the smoothed particle hydrodynamics method (SPH) [Monaghan 1992]. A Real-time sand-water interaction framework has been achieved within the SPH and discrete element method (DEM) [Rungjiratananon et al. 2008].

Authors' address: Xu Wang, wang.xu.lm@alumni.tsukuba.ac.jp; Makoto Fujisawa, fujis@slis.tsukuba.ac.jp; Masahiko Mikawa, mikawa@slis.tsukuba.ac.jp, University of Tsukuba, 1-2 Kasuga, Tsukuba, Ibaraki, Japan, 305-8550.

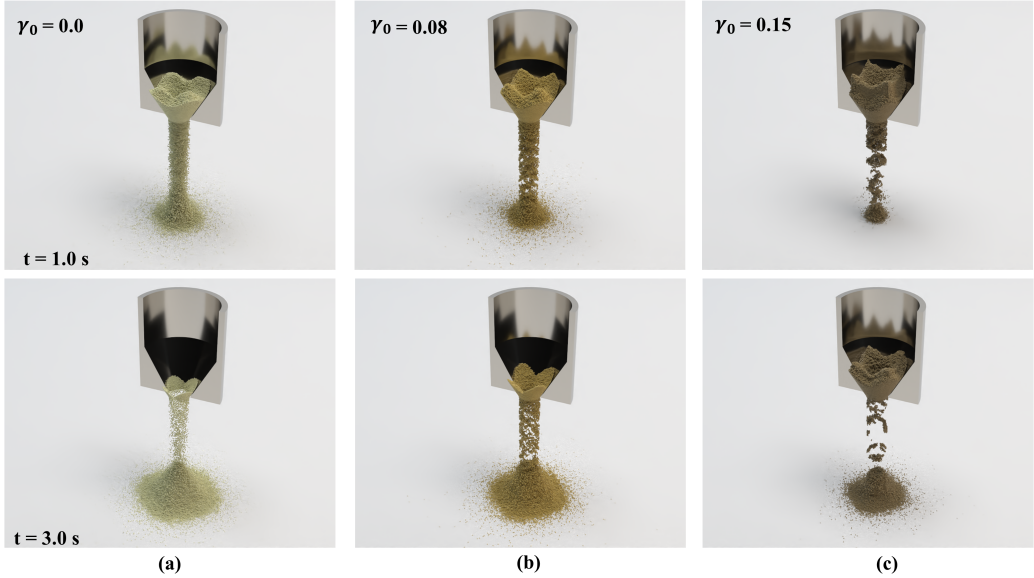


Fig. 2. Soil pouring. (a) The sand-like soil presents its loose features, which enables it to move through the funnel very quickly; (b) The soil with low viscosity has large friction forces between particles and the surface. Some soil particles will attach to the surface of the funnel; (c) The clay-like soil performs a vital cohesiveness characteristic. The large quantity of the soil particles gathers together forming a massive clay, which makes it difficult to pass through the funnel.

Moreover, a porous flow-based approach simulates the interaction between fluids and deformable porous media or granular materials [Lenaerts et al. 2008; Lenaerts and Dutré 2009].

Recent research on intricate interactions between fluids and solids can be divided into two main categories: one is volume fraction based simulations of multi-phase and multi-material flows [Ren et al. 2018], the other is material point method (MPM) based simulations of a mixture of sand and water [Sulsky et al. 1995]. The volume fraction concept was first introduced into the computer graphics community by Müller et al. [2005]. The multiple-fluid framework was proposed by Ren et al. [2014] and Yang et al. [2015] to achieve versatile visual effects based on the mixture model and Helmholtz free energy. Within a few years, Yan et al. [2016] and Yang et al. [2017] extended the multiple-fluid framework to a unified particle system framework that can handle fluid-solid interactions.

In other cases, the MPM has been demonstrated to make realistic visual effects for sand simulations. Tampubolon et al. [2017] achieved the porous sand-water mixture simulation by a semi-implicit two grid MPM, a particle-laden flow simulation solved by a mixed explicit and semi-implicit MPM [Gao et al. 2018]. Simultaneously, the proposed techniques for physically-based simulation of fluids and solids are mainly based on the SPH approach [Koschier et al. 2020], such as snow [Gissler et al. 2020], rigid solids [Gissler et al. 2019], ferrofluids [Huang et al. 2019], viscous fluids [Peer et al. 2015], and elastic solids [Peer et al. 2018]. Although many existing works successfully fulfilled the complicated interactions between multi-phase and multi-material and high degree-of-freedom transitions between sand-like or clay-like soil behaviors and human-made soil structure(e.g., dams, dikes, and embankments) scenarios, failure simulations are seldom seen. In other words, dam breaking similar to disasters caused by overtopping flows or internal seepage erosion is challenging to simulate.

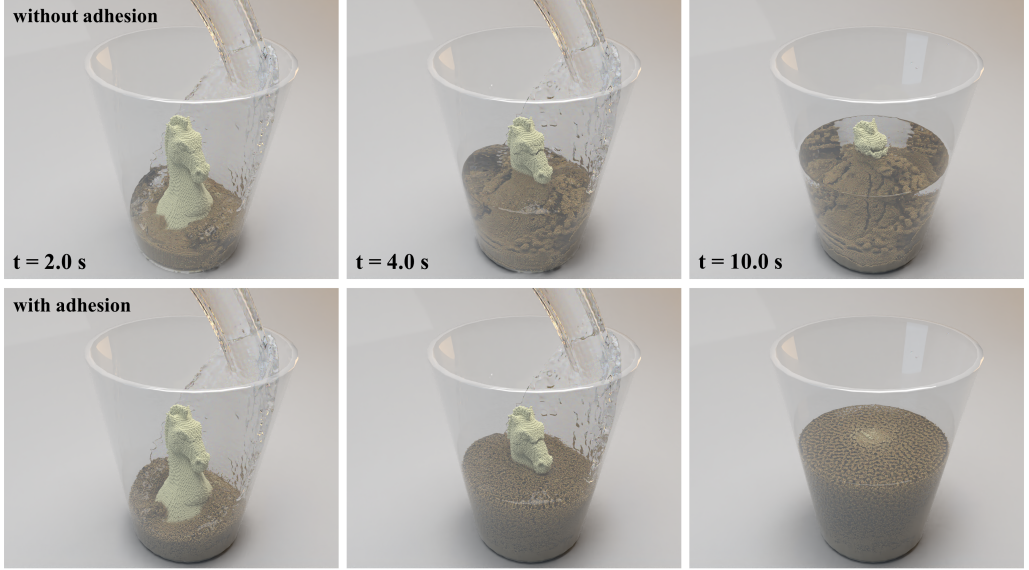


Fig. 3. Sandy chess piece flooded with water. Water pours into a cup and destructs the sandy chess, presenting the effects of our adhesion model. Top row: Without adhesion model the water particles cannot adhere to soil surface, thereby forming sediment due to the capillary forces. Bottom row: With adhesion forces it makes water particles easier adhere to soil particles, reducing their capillary forces.

This paper develops a soil-water coupling method for multi visual effects such as gravity-driven landslides, debris flow, and dam breaking simulations with seepage flows. Also, we use a capillary model to capture various kinds of soil features, e.g., sand-like soils and clay-like soils. Moreover, we resolve the soil particle transitions from dry to wet as water saturation increases. As a result, whether the water smoothly seeps into the soil structures relies on its permeability computed by soil structures' porosity.

The contributions of this paper can be summarized as follows:

- A versatile seepage model is introduced to simulate the effect of water flowing into the soil structure. It is capable of capturing the structural failure phenomena due to the overtopping flow or internal seepage erosion.
- A capillary model for altering the soil behavior can transition sand-like soils to clay-like soils and vice versa, making it easier to keep in a user-specified shape.
- A degree of saturation-based model for soil-water interaction is established: the coefficients of capillary and adhesion base on water saturation, which produce various visual effects for the mixture of soil and water.

2 RELATED WORK

With the rapid development of physical-based simulations, some work adopts the concept of volume fraction to present a mixture of solids and fluids, while others use the MPM to handle the interactions between these two substances. The latter one has recently gained more attention due to its capability of encouraging results. Our work proposes a Lagrangian-Lagrangian framework to reproduce complex internal erosion phenomena based on the seepage flow model. We summarize the previous works related to these topics and briefly introduce some works related to our method.

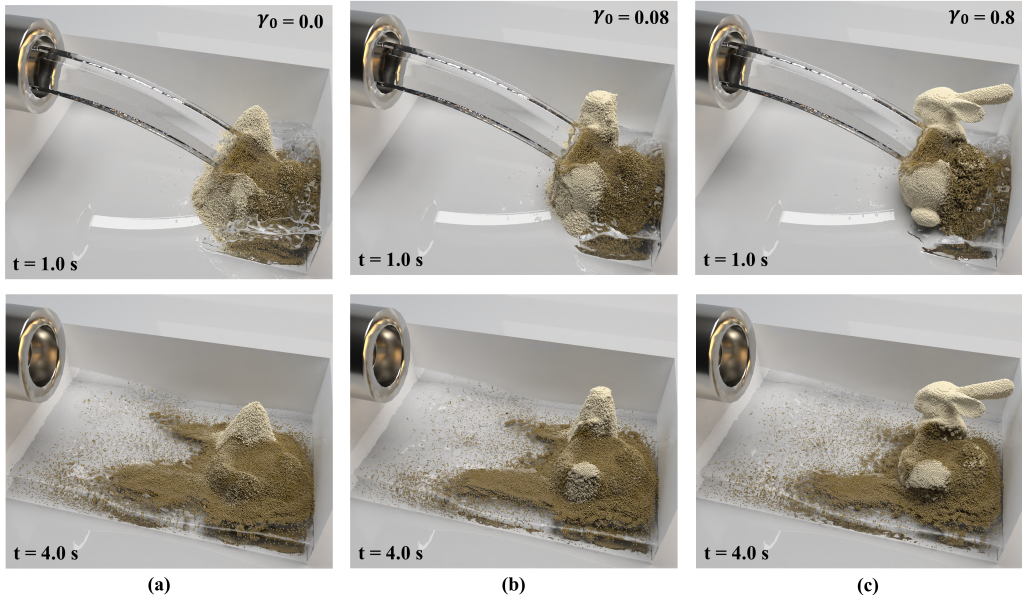


Fig. 4. Destruction of sandy and clay soil structures. Water is poured in from a pipe and destructs the different types of Bunny soil-structure. As water seeps into the soil-structure, its capillary forces decrease. (a): Sand-like soil fails to stay in the shape of Bunny due to their non-cohesiveness behavior. (b): While the soil with a low coefficient of the capillary cannot support the Bunny's shape's integrity, it can retain its outline. (c): Thanks to our capillary model, the clay-like soil can entirely stay the shapes of Bunny.

Volume Fraction Based Approaches. To simulate various phenomena of fluid-fluid interactions, a dynamic phase transitions model was proposed by Müller et al. [2005]. Nielsen and Østerby [2013] utilized the air-water volume fraction model to simulate phase transitions, making water spray simulation possible. Ren et al. [2014] extended the two-phase flow model to a multiple fluid mixture model. An energy-based fast multiple fluid model is presented by Yang et al. [2015]. Additionally, the volume fraction model can also be implemented in the MPM [Yan et al. 2018] framework and implicit incompressible SPH [Jiang et al. 2020] framework to simulate the miscible and immiscible fluids. As for the interactions between solid and liquid, Yan et al. [2016] extended the mixture model introduced by Ren et al. [2014], improving the phase transitions between solids and fluids. Yang et al. [2017] introduced a unified particle system framework, which can simulate the multi-phase and multi-material visual effects. Although these approaches well achieved multi-material visual effects and the mixture of granular materials and water, they took no account of internal erosion phenomena, which is reconsidered in our seepage flow model.

MPM for Sand-Water Mixture. Recently, the development of MPM has been advanced due to its visual plausibility on elastoplastic and granular materials simulations [Fu et al. 2017; Hu et al. 2018; Jiang et al. 2017, 2015, 2016]. Previous works have also solved the interactions between granular materials and water. A sand-water mixture framework is implemented by the semi-implicit two grid MPM [Tampubolon et al. 2017]. Besides, a mixed explicit and semi-implicit MPM solver has been proposed to simulate the particle-laden flow [Gao et al. 2018]. Concretely, Tampubolon et al. [2017] focused on the landslides and debris flows that are similar to our simulation scenarios. The model they adopted can simulate internal seepage erosion and achieve the overtopping flow scenarios mild extension. However, they used the MPM approach, whereas we use a particle-based SPH-DEM system for soil-structure destruction visual simulation. Unlike particle-laden flow by Gao

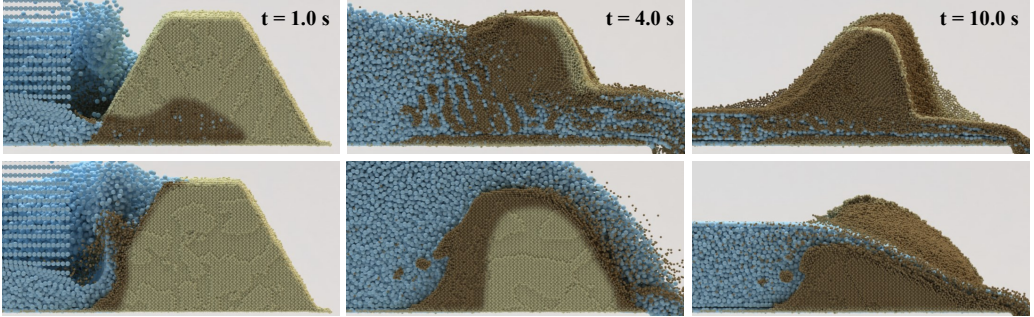


Fig. 5. Cross section of dam breaking in Figure 9.

et al. [2018], which can simulate sediment transport, sedimentation, our model focus on different types of soil-structure destruction due to internal seepage erosion.

Sand-Fluid Interaction. Rungjirathananon et al. [2008] introduced the SPH-DEM coupling framework to simulate the sand with wetting effects. Their wetness propagating method uses isotropic diffusion to realize the wetness values transferred between sands by absorbing water particles. In contrast, we develop a seepage model that considers sand particles' void ratio as a significant factor for anisotropic diffusion between sands. While the granular materials as the porous flow [Lenaerts and Dutré 2009] can easily simulate the dry sand to mud behavior, the granular particles' permeability is neither easily controlled nor suitable for overtopping flow simulations.

Multi-Scale Model. Fei et al. [2017] proposed a multi-scale model-based framework for liquid-hair, liquid-fabric [Fei et al. 2018], and shear-dependent liquids-strands simulation [Fei et al. 2019]. Their works adopted an empirically validated drag model and a surface tension-induced cohesion model for simulating the interactives between materials with surrounding fluid volume, which are similar to our seepage model and capillary model. However, our framework can compute the drag forces between the fluid particles and surrounding soil particles and allow fluid particles to seepage into soil structures for observing the infiltration situation. As for our capillary model, extra fluid particles will not be configured in soil structures. Instead, we assume that there is a small fixed volume of liquid bridge between soil particles. Only when the actual fluid particles seepage into soil structures can cohesion forces between the soil particles dynamically change.

SPH-DEM Coupling. SPH-DEM coupling method is commonly used in engineering literature works for fluid-solid interaction(FSI), such as seepage flows [Harasaki and Asai 2016], landslide and surge waves [Tan and Chen 2017], and granular flows [Daviet and Bertails-Descoubes 2017] simulations. Other engineering literature works utilized the seepage force for coupled flow deformation analysis [Bui and Nguyen 2017] or fluid-granular interaction analysis [Xu et al. 2019]. Several attempts have been made to simulate the solids, such as coupling discrete elements and then couple them with liquid computed by the drag force(seepage force)[Sun et al. 2013; Zhou et al. 2010]. On this basis, a non-spherical DEM particulate system for particle-fluid flow was developed by Zhong et al. [2016]. A computational fluid dynamics solver for internal seepage erosion simulation was proposed by Xiao and Wang [2020]. In contrast to these approaches, which mainly focus on numerical precision and analysis, our work brings up a novel SPH-DEM visual simulation framework with a water saturation-based capillary model and adhesion model to capture the wide range of soil-water mixture phenomena.

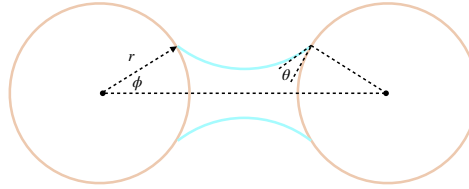


Fig. 6. Liquid bridge between two soil particles.

3 SOIL MATERIAL SIMULATION

In this section, we describe a capillary model based on the DEM method. It is capable of simulating sand-like or clay-like soil behavior materials. The clay-like material plays an essential role in affecting structural failure, which is hard to deal with the standard DEM. In describing the physical models, our notation uses subscripts i, j to indicate the fluid particles related to the seepage flow model and k for soil particles related to our capillary model.

3.1 Discrete Element Model

DEM is a Lagrangian-based simulation model for granular medium, widely used in soil mechanics-related fields [Cundall and Strack 1979]. Each particle k in the DEM system is a rigid body with position \mathbf{x}_k and radius r_k . When the distance $d = \|\mathbf{x}_{k_1 k_2}\| < r_{k_1} + r_{k_2}$ between particle k_1 and k_2 (two DEM particles penetrate with each other), the normal force \mathbf{F}_k^n and tangential force \mathbf{F}_k^t acting on particle k , define as [Hentz et al. 2004]:

$$\begin{aligned}\mathbf{F}_k^n &= K_N(r_{k_1} + r_{k_2} - d) \frac{\mathbf{x}_{k_1 k_2}}{\|\mathbf{x}_{k_1 k_2}\|} \\ \mathbf{f}_k^t &= -K_T(\mathbf{v}_{k_1 k_2} - \mathbf{v}_{k_1 k_2} \cdot \frac{\mathbf{x}_{k_1 k_2}}{\|\mathbf{x}_{k_1 k_2}\|}) \\ \mathbf{F}_k^t &= \begin{cases} \frac{\|\mathbf{F}_k^n\| \tan \varphi}{\|\mathbf{f}_{k_2}^t\|} \mathbf{f}_{k_2}^t & (\|\mathbf{f}_{k_2}^t\|^2 > (\|\mathbf{F}_k^n\| \tan \varphi)^2) \\ \mathbf{f}_{k_2}^t & (\text{otherwise}) \end{cases}\end{aligned}$$

where K_N is the normal stiffness coefficient related to Young's modulus Y , K_T is the tangent stiffness coefficient related to the Poisson's ratio ν , φ is the friction angle, and $\mathbf{x}_{k_1 k_2} = \mathbf{x}_{k_1} - \mathbf{x}_{k_2}$, $\mathbf{v}_{k_1 k_2} = \mathbf{v}_{k_1} - \mathbf{v}_{k_2}$.

3.2 Capillary Action

Capillary action, enabling the soil to retain a small amount of water, is more commonly seen in the porous media. From a microscopic point of view, water between soil particles forms a liquid bridge due to the surface tension of the liquid. As a result, the liquid bridge induces attractive forces between soil particles, which play a vital role in representing the behavior of natural or human-made soil structures. Rungjirathanon et al. [2008] computed the wetness of granular materials by the liquid bridge based on the amount of wetness stored in the sand particles to compute the liquid bridge forces. In contrast, we adopt a total energy theory [Rabinovich et al. 2005] to capture the capillary action between the soil particles, which aims to keep soil structures stable without any actual water particles.

3.2.1 Total energy based capillary force. A liquid bridge is usually formed on the solid surface, which is induced by the surrounding vapor; it can spontaneously condense to the liquid and attach to the surface of the solid. As for estimating the capillary forces between two solid surfaces,

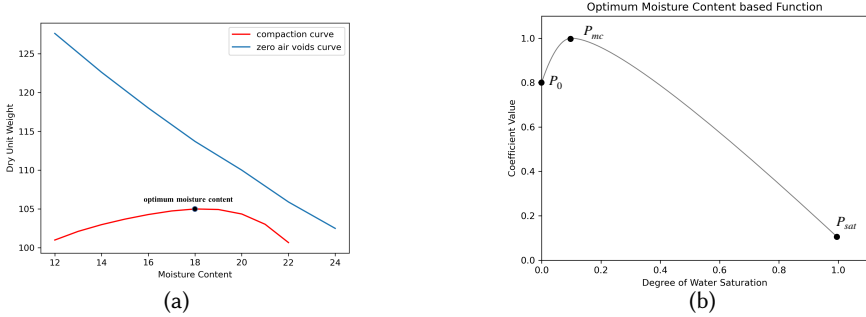


Fig. 7. (a) **Compaction curve and zero air voids curve** illustrated from laboratory data [Kaliakin 2017]. (b) **Composite Bézier curve**. A composite Bézier curve for optimum moisture content based function $\Gamma(\cdot)$. In this example, we set $\gamma_0 = 0.8$, $S_{mc} = 0.1$, $\gamma_{mc} = 1.0$ and $\gamma_{sat} = 0.1$.

Rabinovich et al. [2005] considered that not only the energy of the solid surface under the liquid bridge is indispensable, the energy of the liquid bridge itself (meniscus energy term) should also be taken into account. Moreover, they provide experimental measurements that have verified this method's effectiveness by atomic force microscope (AFM). Therefore, we extend this method to the DEM and use the optimum moisture content curve to manipulate the effect of capillary forces. Notably, the total energy theory can only be established when the liquid bridge volume V_{lb} is of a low constant value. The dimensionless capillary force between two spherical particles is given by Rabinovich et al. [2005]:

$$F^{cp} = f^{cp,sf} + f^{cp,men} \quad (1)$$

$$f^{cp,sf} = -\frac{2\pi\gamma r \cos(\theta)}{1 + \frac{H}{-H + \sqrt{H^2 + \frac{V_{lb}}{\pi r}}}} \quad (2)$$

$$f^{cp,men} = -2\pi\gamma r \sin(\phi) \sin(\phi + \theta) \quad (3)$$

In this equation, the meniscus energy term $f^{cp,men}$ represents the vertical component of the liquid bridge surface tension [De Lazzer et al. 1999]. And surface energy term $f^{cp,sf}$ can be derived by the energy of the solid surface under the liquid bridge [Israelachvili 2011], and we provide the detailed derivation in Appendix A.1:

$$E = -2\pi\gamma r^2 \phi^2 \cos(\theta) \quad (4)$$

where γ is the surface tension, r is the particle radius, θ is the contact angle. H is the distance between two soil particles. And ϕ is the half-filling angle as shown in Fig 6 which can be computed by:

$$\phi = \sqrt{\frac{H}{r} \left(-1 + \sqrt{1 + \frac{2V_{lb}}{\pi r H^2}} \right)} \quad (5)$$

Liquid bridge volume V_{lb} is 0.1% of the fluid particle volume. Figure 6 illustrates the liquid bridge between two soil particles.

3.2.2 Compaction curve based capillary model. In order to achieve the stable human-made soil-structure simulation, we assume that there is a virtual small fixed volume of liquid bridge between soil particles. Since the soil particles do not interact with actual fluid particles, we assign the liquid bridge volume to a fixed small value when computing the capillary forces between soil particles in Equation 1. As for soil particles interacting with actual fluid particles, despite the volume of fluid-particle $V_i \gg V_{lb}$, we regard the soil-fluid interaction as a compactive-effort-like behavior, which can reproduce the soil-structure destruction scenarios. Since soil compaction plays a vital role in human-made structures construction, either lower water contents or higher water contents will cause the destruction of structures [Yusoff et al. 2017]. Thus, we take the compaction curve into our capillary model, which means that the stability of soil structures can only be maintained at the optimum moisture content point(maximum capillary force). The relationship between the moisture content and dry unit weight is illustrated in Fig.7a by laboratory data [Kaliakin 2017], compared with the zero air voids curve and the compaction curve. In order to adjust the visual effect of soil-structure destruction, we propose a composite Bézier function $\Gamma(\cdot)$ (Fig.7b) to dynamically adjust the coefficient based on the optimum moisture content curve. Additionally, one should consider that when the distance between two soil particles exceeds rupture distance d_{rup} , the liquid bridge will be stretched to break in apart. With respect to the separation distance, Lian et al. [1993] discovered the property that the rupture distance is proportional to the cube root of the liquid bridge volume. Following this phenomenon, Willett et al. [2000] proposed a more precise approximation formula for determining the rupture distance in liquid bridges between particles of different size. Since our framework only supports equal particle radii, we use a revised equation of the rupture distance [Willett et al. 2000] to constrain the capillary model, as follows:

$$d_{rup} = (1 + 0.5\theta)(V_{lb}^{\frac{1}{3}} + 0.1V_{lb}^{\frac{2}{3}}) \quad (6)$$

As for implementing the capillary model in our framework, only if the distance d between two particles is less than the d_{rup} and does not penetrate with each other, the capillary forces can be accounted into our framework. Combined with the concept of rupture distance d_{rup} ; our compaction curve based capillary model is defined as:

$$F_k^{cp} = \begin{cases} -\Gamma(S_k^r)(f^{cp,men} + f^{cp,sf}) \frac{\mathbf{x}_{k_1 k_2}}{\|\mathbf{x}_{k_1 k_2}\|} & 0 < H < d_{rup} \\ 0 & (\text{otherwise}) \end{cases} \quad (7)$$

where S_k^r is the saturation degree of particle k , $\Gamma(\cdot)$ is the optimum moisture content based function that created by a composite Bézier curve, which is controlled by three points $P_0(0, \gamma_0)$, $P_{mc}(S_{mc}, \gamma_{mc})$, and $P_{sat}(1, \gamma_{sat})$. γ_0 presents the initial capillary coefficient at the initial degree of saturation, γ_{sat} is the capillary coefficient of soil at the fully saturated situation, γ_{mc} is a user-defined capillary coefficient of soil at the optimum moisture content S_{mc} . Specifically, γ_0 plays an essential role in the simulation of stable soil structures, but an excessive capillary force may trigger unnatural physical phenomena. Thus in our work, γ_0 varies between 0.6 to 0.9, γ_{mc} is around 0.8 to 1.0, and γ_{sat} is around 0.0 to 0.1 (should not exceed the value of γ_0). Figure 7b displays a composite Bézier curve which is typically used in our experiments.

4 SEEPAGE FLOW SPH SIMULATION

Our seepage flow model is based on the SPH methods widely used in fluid simulation due to their efficiency and straightforward implementation. By introducing the seepage force and buoyancy force into the SPH momentum equation, we develop an SPH framework for simulating the effect of water flowing into the soil structure. In this section, we will briefly introduce the foundations of our seepage flow model.

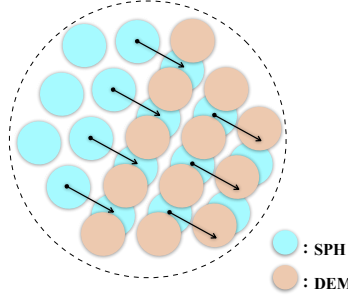


Fig. 8. Seepage flow in particle view. In our SPH-DEM framework, the water particles can smoothly pass through the soil structures constructed by the soil particles. The blue and brown particles respectively represent the SPH and DEM particles.

4.1 SPH fluid simulation

SPH is a Lagrangian-based simulation method that was proposed initially for astrophysics simulations [Lucy 1977]. A constant property $\phi(\mathbf{x})$ can be approximated by interpolating between the respective property values around the point \mathbf{x} [Monaghan 1992] using the following formula:

$$\phi(\mathbf{x}) = \sum_{j \in N} \phi_j \frac{m_j}{\rho_j} W_{ij}(\mathbf{x}_i - \mathbf{x}_j, h)$$

where ϕ_j is the continuous property value at particle j , N is a set of neighboring particles, m_j is the mass of particle j , ρ_j is its density, W_{ij} is a kernel function with smoothing radius h which the $\sum_j \frac{m_j}{\rho_j} W_{ij} = 1$ should be satisfied. And $\mathbf{x}_i, \mathbf{x}_j$ respectively represent the position of particle i, j .

4.2 Seepage Flow Model

The seepage flow mainly occurs in water flowing through the soil structures when there is a difference in water levels on the two sides. The behavior of the saturated soils is determined by the interactions between the soil structure and the water. A mixture theory for drag and buoyancy terms was initially proposed by Anderson and Jackson [1967]. Then Bowen [1976] used momentum exchange terms for handling the mixture of elastic fluid(gas) and porous soil media. Bui and Nguyen [2017] adopted the momentum exchange terms for computing the force acting on the fluid phase due to the soil structure, as follows:

$$\mathbf{R} = \underbrace{-\frac{\gamma_w(1-n_w)^2}{C_k n_w} (\mathbf{v}_w - \mathbf{v}_s)}_{\text{drag term}} - \underbrace{n_s \nabla p_w}_{\text{buoyancy term}} \quad (8)$$

where γ_w is the unit weight of water, n_w is the volume fraction of water, n_s is the volume fraction of soil, C_k is the Kozeny–Carman’s constant from laboratory test [Bear and Cheng 2010], \mathbf{v}_w and \mathbf{v}_s respectively represent the velocity of soil and water in the porous medium. In our method, we use an average water velocity \bar{v}_k which is around the soil particle k to replace the computation of \mathbf{v}_w , as follows:

$$\bar{v}_k = \frac{\sum_j \mathbf{v}_j V_j W_{kj}}{\sum_j V_j W_{kj}} \quad (9)$$

Bui and Nguyen [2017] derived the momentum exchange term for seepage flow and came up with a continuum theory, whereas we develop an SPH-DEM framework aiming to capture various

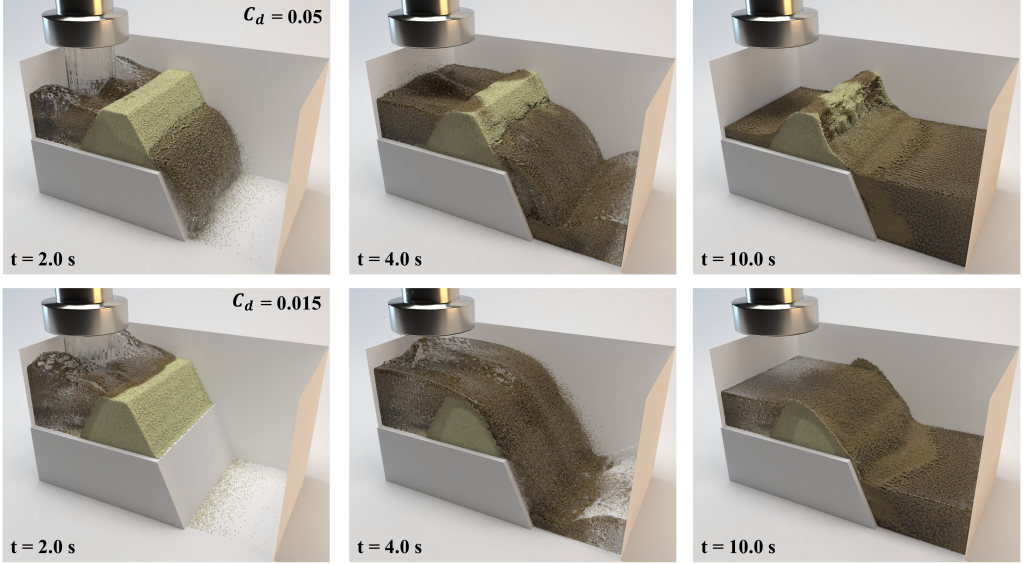


Fig. 9. Dam breaking. Here we present two different destruction types of soil structures related to our drag coefficient C_d . Top row: Dam breaking scenario caused by internal seepage erosion with a low drag coefficient. Bottom row: Based on the capillary model and a high drag coefficient, we can easily simulate the dam breaking under the overtopping flow.

soil behaviors. Specifically, Figure 8 shows the SPH particles can smoothly pass through the soil-structure(assembled by DEM particles), which gives drag and buoyancy force to DEM particles and receives the symmetric forces from DEM particles. Thus, we can utilize the porosity of particles for replacing the void fraction of water n_w in Equation(8). Despite the $\sum_j V_j W_{ij} = 1$ already known in SPH approximation, the volume fraction value of water particle i can be defined as:

$$n_i = 1 - \sum_k V_k W_{ik} \quad (10)$$

where V_k is the volume of soil particle k , and n_i is the volume fraction of water particle i .

The drag term in Equation(8) relies not only on the relative velocity of water but the local density of neighboring solid particles should also be taken into account, and the latter can be captured by the average local voidage [Sun et al. 2013]:

$$n_k = \frac{\sum_j n_j V_j W_{jk}}{\sum_j V_j W_{jk}} \quad (11)$$

In order to manipulate the seepage rate, we use the coefficient of drag force C_d to replace the Kozeny–Carman’s constant in the drag term part of Equation(8). The drag term in Equation(8) for soil particles k can be expressed as:

$$\mathbf{F}_k^d = -\frac{\gamma_w (1 - n_k)^2}{C_d n_k} (\bar{\mathbf{v}}_k - \mathbf{v}_k) \quad (12)$$

According to Newton’s third law of motion, the reactions of the drag force acting on the soil particles are defined as a portion of the drag force proportional to the weight of water particles.

Thus the symmetric drag force from a soil particle to a water particle F_i^d can be written as:

$$F_i^d = \sum_k \frac{F_k^d}{\sum_j V_j W_{kj}} V_i W_{ik} \quad (13)$$

Notably, the average drag force for soil particle k should be computed first.

The buoyancy term in Equation(8) for soil particle k can be derived by the thermal energy, which is similar to the Hamiltonian framework [Price 2012]:

$$F_k^b = -V_k \sum_j \frac{m_j}{\rho_j} p_j \nabla W_{jk} \quad (14)$$

Similar to Equation(12), buoyancy is also an interactive force acting between solid and liquid. Therefore, the symmetric buoyancy force of Equation(14) from a soil particle to a water particle can be written as:

$$F_i^b = -\frac{m_i}{\rho_i} p_i \sum_k V_k \nabla W_{ki} \quad (15)$$

4.3 Saturation-based Adhesion Model

While in Section 3.2, we describe a capillary model for soil particles, the assumption of total energy theory is the volume of the liquid bridge being of a fixed constant value. That means the capillary model is unable to achieve the molecular interaction between soil and sand particles. We adopt the fluid-solid adhesion model proposed by Akinci et al. [2013], who use a steep parabolic function, to produce robust and attractive forces gathering fluid particles in the SPH kernel, as follows:

$$F_i^a = m_i \sum_k \Gamma(n_k) m_k A_{ik} \frac{\mathbf{x}_{ik}}{\|\mathbf{x}_{ik}\| + \eta} \quad (16)$$

where $A(\cdot)$ is a spline function that created by SPH [Akinci et al. 2013]:

$$A(r) = \begin{cases} \frac{0.007}{h^{3.25}} \sqrt{\frac{-4r^2}{h} + 6r - 2h} & 2r > h \wedge r \leq h \\ 0 & (\text{otherwise}) \end{cases}$$

As for $\Gamma(\cdot)$, we use a similar composite Bézier curve(Figure 7b) to replace the adhesion coefficient in Akinci et al. [2013], but we need another set of coefficients to define the optimum moisture content based function. β_0 presents the initial adhesion coefficient at the initial degree of saturation, β_{sat} is the adhesion coefficient of soil at the fully saturated situation, β_{mc} is a user-defined adhesion coefficient of soil at the optimum moisture content S_{mc} .

As for soil particles k , we use a similar strategy in Equation(12), the symmetric adhesion force can be expressed as:

$$F_k^a = \sum_j \frac{F_j^a}{\sum_{k'} V_{k'} W_{jk'}} V_k W_{kj} \quad (17)$$

where k' presents the the neighboring soil particles of soil particle k .

4.4 Implementation

Algorithm Framework. The implementation of our method uses weakly incompressible WC-SPH [Becker and Teschner 2007] for liquid simulation and DEM [Cundall and Strack 1979] for granular simulation. Since our seepage flow based SPH-DEM framework mainly focuses on handling the interactions between water and soil particles, it is possible to integrate our framework with incompressible methods directly, likes PCISPH [Solenthaler and Pajarola 2009], IISPH [Ihmsen et al. 2013], or DFSPH [Bender and Koschier 2015]. As drag term, capillary term, and adhesion term



Fig. 10. Multiple failure modes of the dam in a valley. Here we show an example of different dam materials resulting in different failure modes in the floods. Three individual dams with respective drag coefficient are setted up in a valley. Right dam: An unstable structure with high permeability, which can be easily washed away by floods; Middle dam: A stable structure with low permeability making it only broken down by overtopping flows; Left dam: A stable structure with high permeability is finally destructed by internal seepage erosion.

are not directly related to pressure, they can be treated as external forces, and the buoyancy term acting on the soil particles depends on the pressure of the surrounding water particles. In the case of method IISPH, the computation of the buoyancy term has to be performed after pressure solver.

As for the boundary handling, we use the particles obtained by sampling the surface of rigid objects as boundary particles. To ensure that SPH particles near the boundary do not reproduce the clustering and penetrating problems, we implemented the Akinci et al. [2012] method in our framework. In addition, when calculating the interaction between DEM particles and boundary particles, we only need to regard the boundary particles as DEM particles directly and without modifying any parameters.

Moreover, our framework can be easily implemented in GPU for parallelization. For finding neighboring particles, we employed a spatial subdivision technique described by Green [2010], and we chose the SPH smoothing length h as $4r$. It is worth noting that each particle of soil and water should be labeled as a different group to avoid incorrect neighbor searching. For all scenes in our experiments, water particles that have a rest density of 1000. As for soil particles, with a rest density of 2700, Young's modulus $Y = 1e^5$, Poisson's ratio $\nu = 0.3$, and friction angle $\varphi = 0.5$. All algorithms, including the capillary and seepage and adhesion models, are summarized in the supplemental document.

Time Stepping. The Rayleigh criterion is implemented in our framework for determining the time step of soil particles, which is based on the energy that cannot propagate from a particle to its neighbors in a single time step [Tavarez and Plesha 2007]. Similar to Burns et al. [2019], the Rayleigh timestep can be described by:

$$\Delta t_{soil} = \frac{\pi \min(r_k)}{\beta} \sqrt{\frac{\rho}{Y}} \quad (18)$$

$$\beta = 0.8766 + 0.163\nu$$

As for the time step of fluid particles, we adopt the method proposed by Goswami and Batty [2014]:

$$\Delta t_{fluid} = \min \left\{ \frac{\lambda_0 r}{c_s}, \lambda_f \sqrt{\frac{rm}{F_{max}}} \right\} \quad (19)$$

Then we choose the smaller Δt computed from Equation(18) and Equation(19) as the final time step for our framework.

Table 1. Performance for our experiments

Experiment	sec/step	steps/frame	max Δt	max SPH particles	total particles
Example 1	0.13	202	1.6×10^{-4}	0	80k
Example 2	0.14	81	4.0×10^{-4}	200k	520k
Example 3	0.14	81	4.0×10^{-4}	140k	500k
Example 4	1.19	81	4.0×10^{-4}	300k	1.4m
Example 5	1.05	81	4.0×10^{-4}	420k	1.8m

We have implemented our framework on an NVIDIA GeForce RTX2080Ti 12GB GPU. We used Houdini to reconstruct the fluid surface, and images were rendered with Redshift. Our experiments in Section 5 typically run at time steps between 1×10^{-4} and 1×10^{-5} . Table 1 records the performance of our SPH-DEM framework for the experiments shown here.

5 RESULTS

This section briefly describes various experiments to demonstrate our framework, which captures a wide range of phenomena for the soil-water mixture. The critical value of parameters used in our experiments can be found in Table 2.

Example 1:Soil pouring. Figure 2 demonstrates the capacity of the capillary model for capturing the realistic sand-like and clay-like soil behaviors. In Figure 2(a), the sand-like soil presents its loose features when poured quickly through the funnel. Whereas in Figure 2(b), we utilize the capillary model with a low surface tension coefficient, the soil particles have a low viscosity, and some of the soil particles attach to the surface of the funnel. As shown in Figure 2(c), the clay-like soil performs a vital cohesiveness characteristic. As a result, the large quantity of the soil particles gathers together to form a massive clay, making it difficult to pass through the funnel.

Example 2:Sandy chess piece flooded with water. Figure 3 simulates sandy chess piece destruction caused by water poured into a cup. In this example, we compare two visual effects of the soil-water mixture under different coefficients of the adhesion model. Figure 3(Top row) shows that the water particles cannot adhere to the soil particles' surface without the adhesion model. As a result, the bulk of the soil particles have large capillary forces in forming the sediments. The adhesion model in Figure 3(Bottom row) presents that the water particles can easily adhere to soil particles and reduce the cohesive forces.

Example 3:Destruction of sandy and clay soil structures. In Figure 4, three different types of Bunny soil structures are destructed by the pouring water. As water seeps into the soil structure, it decreases the capillary forces between soil particles. The top row in Figure 4 presents the sand-like soil that cannot stay in the shape of Bunny due to its non-cohesiveness behavior. The middle row shows the effect of soil particles with a low coefficient of surface tension. Thanks to our capillary model, the bottom row in Figure 4 displays that the clay-like soil can entirely stay the shapes of Bunny.

Example 4:Dam breaking. Figure 9 demonstrates different types of dam-breaking simulations. A lower drag coefficient in the seepage model usually leads to a higher seepage water flow rate in soil structures, while a higher drag force can strongly resist the seepage flow. As shown by the top row in the 9, the soil structure is steadily eroded by the water internally. The bottom row reproduces the overtopping flow disaster. In contrast to the volume fraction-based frameworks [Yan et al. 2016; Yang et al. 2017], our framework represents the infiltration situation of fluid in soil-structures (Figure 5) and realizes different destruction types of granular material-based structures simulation

(Figure 9). Unlike the dissolution process-based fluid-granular mixture effect in Yan et al. [2016]; Yang et al. [2017], we reproduce the fluid-granular mixturing scenarios through seepage process.

Example 5:Multiple failure modes of the dam in a valley. In Figure 10, different materials of the dam result in different failure modes in the floods. The right side dam is designed to be an unstable structure with high permeability, which floods can easily wash away; the middle one is stable with low permeability but can be destroyed by overtopping flows; the left one has high permeability with a stable structure that is finally destructed by internal seepage erosion.

6 DISCUSSION AND FUTURE WORK

We have developed a soil-water coupling framework to simulate the phenomena of soil-structure destruction. A variety of experiments on destruction simulation have made it simpler and more comfortable implementing the novel approach, which can capture multiple visual effects, including wet granular materials, clay-like soil simulation, and soil-structures destruction, as shown in the experiments above.

Our method uses a water saturation-based capillary model and adhesion model for resolving the interactions between soil and water. We only need to assign an optimum moisture content curve to compute the capillary and adhesion models' coefficients. This approach can be implemented in other SPH frameworks for soil-water mixture simulation. However, it does not take into account the chemical reaction between the soil particles and water particles. As a result, it is possible to capture the effect of water particles attached to soil particles' surface, but the phenomena like the dissolution of soils in Yang et al. [2017] is not included, and the non-Newtonian fluid which caused by miscible soil-water in our framework has not been taken.

Although our capillary model can alter the behavior of soil particles, rendering the high resolution of soil particles will reduce the maximum timestep. Thus, the computation cost and computation time will be significantly increased and even more than the hybrid methods. Other than that, since the capillary force model cannot detect whether the soil particles are underwater or not, an artificial phenomenon similar to "spherical clumps" is observed in our experiment. Because the water content of soil particles is related to the volume of surrounding water particles, especially those located near the central part of the "spherical clumps", their water content can not be computed correctly. We have attempted to resolve this issue using more significant adhesion coefficients as in Figure 3 (Bottom row). However, a larger selection of coefficients may cause the wet soil particles to be uniformly distributed into the water rather than settling near the bottom. In the future, we would like to resolve this artificial phenomenon without the requirement of parameter tuning.

The seepage flows are represented in our framework by linear drag term and buoyancy term, which can easily control seepage rate and soil permeability. However, the porosity of particles is inaccurate in our framework due to the unified radius particle. In the future, we prefer to use multi-radius particles and non-spherical particles as parts of our soil structures for attaining a more accurate porosity. While our dam breaking example presents the effectiveness of our linear drag term, the linear drag term cannot be applied to turbulent scenarios, which need to be discussed in further research. Furthermore, we would like to improve our framework's performance, significantly reducing the cost of computation dealing with the high resolution of soil particles. Lastly, we hope to capture non-Newtonian fluid phenomena (e.g., debris flows) and chemically reaction interactions between soil and water in our future works.

ACKNOWLEDGMENTS

We would like to thank the anonymous reviewers for their valuable suggestions and comments. This work was supported by JSPS KAKENHI Grant Number JP20K11839.

Table 2. Table of parameters

Experiment	$\gamma_0/\gamma_{mc}/\gamma_{sat}$	$\beta_0/\beta_{mc}/\beta_{sat}$	C_d
Example 1	(0.0, 0.08, 0.15)/−/−	−	−
Example 2	0.8/1.0/0.1	(−, 2.0)/(−, 2.2)/(−, 1.0)	0.1
Example 3	(0.0, 0.08, 0.8)/1.0/0.1	1.0/1.2/0.3	0.05
Example 4	0.6/1.0/0.1	1.0/1.2/0.3	(0.015, 0.05)
Example 5	0.6/1.0/0.1	1.0/1.2/0.3	(0.02, 0.015, 0.05)

A APPENDIX

A.1 APPENDIX A. Derivation of Equation(2)

This appendix shows the detailed derivations of Equation(2). The adhesion force between two spherical particles or two planar bodies can be computed by the Derjaguin approximation [Israelachvili 2011], which is related to the interaction free energy $E(H)$ is given by:

$$F(H) = -\frac{dE}{dH} \quad (20)$$

In order to compute the surface energy term of liquid bridge, we substitute Equation(4) to Equation(20). Surface tension force between two spheres with a liquid bridge can be expressed as:

$$f^{cp,sf} = -\frac{dE}{dH} = 4\pi\gamma r^2\phi \cos(\theta)\frac{d\phi}{dH} \quad (21)$$

The volume of liquid bridge can be approximately computed by geometrical method [Rabinovich et al. 2005] as follows:

$$V_{lb} = \pi r^2 \phi^2 H + \frac{1}{2}\pi r^3 \phi^4 \quad (22)$$

Despite that the volume of liquid bridge is a fixed value in total energy theory, $\frac{dV_{lb}}{dH} = 0$, substituted by Equation(22):

$$\frac{d\phi}{dH} = -\frac{1}{\frac{2H}{\phi} + 2r\phi} \quad (23)$$

Combine Equation(5), Equation(21) and Equation(23), it leads to result of the right-hand side of Equation(2).

REFERENCES

- Nadir Akinci, Gizem Akinci, and Matthias Teschner. 2013. Versatile surface tension and adhesion for SPH fluids. *ACM Transactions on Graphics (TOG)* 32, 6 (2013), 1–8.
- Nadir Akinci, Markus Ihmsen, Gizem Akinci, Barbara Solenthaler, and Matthias Teschner. 2012. Versatile rigid-fluid coupling for incompressible SPH. *ACM Transactions on Graphics (TOG)* 31, 4 (2012), 1–8.
- T. B. Anderson and Roy Jackson. 1967. Fluid Mechanical Description of Fluidized Beds. Equations of Motion. *Industrial & Engineering Chemistry Fundamentals* 6, 4 (1967), 527–539. <https://doi.org/10.1021/i160024a007>
- Jacob Bear and Alexander H-D Cheng. 2010. *Modeling groundwater flow and contaminant transport*. Vol. 23. Springer Science & Business Media.
- Markus Becker and Matthias Teschner. 2007. Weakly compressible SPH for free surface flows. In *Proceedings of the 2007 ACM SIGGRAPH/Eurographics symposium on Computer animation*. 209–217.
- Jan Bender and Dan Koschier. 2015. Divergence-free smoothed particle hydrodynamics. In *Proceedings of the 14th ACM SIGGRAPH/Eurographics symposium on computer animation*. 147–155.
- Ray M. Bowen. 1976. *Theory of Mixtures. Continuum Physics*. Butterworth-Heinemann. 1–127 pages.
- Ha H Bui and Giang D Nguyen. 2017. A coupled fluid-solid SPH approach to modelling flow through deformable porous media. *International Journal of Solids and Structures* 125 (2017), 244–264.
- Shane J Burns, Petri T Piironen, and Kevin J Hanley. 2019. Critical time step for DEM simulations of dynamic systems using a Hertzian contact model. *Internat. J. Numer. Methods Engrg.* 119, 5 (2019), 432–451.

- Peter A Cundall and Otto DL Strack. 1979. A discrete numerical model for granular assemblies. *geotechnique* 29, 1 (1979), 47–65.
- Gilles Daviet and Florence Bertails-Descoubes. 2017. Simulation of Drucker–Prager granular flows inside Newtonian fluids. (2017).
- A De Lazzer, M Dreyer, and HJ Rath. 1999. Particle–surface capillary forces. *Langmuir* 15, 13 (1999), 4551–4559.
- Yun Fei, Christopher Batty, Eitan Grinspun, and Changxi Zheng. 2018. A multi-scale model for simulating liquid-fabric interactions. *ACM Transactions on Graphics (TOG)* 37, 4 (2018), 1–16.
- Yun Fei, Christopher Batty, Eitan Grinspun, and Changxi Zheng. 2019. A multi-scale model for coupling strands with shear-dependent liquid. *ACM Transactions on Graphics (TOG)* 38, 6 (2019), 1–20.
- Yun Fei, Henrique Teles Maia, Christopher Batty, Changxi Zheng, and Eitan Grinspun. 2017. A multi-scale model for simulating liquid-hair interactions. *ACM Transactions on Graphics (TOG)* 36, 4 (2017), 1–17.
- Chuyuan Fu, Qi Guo, Theodore Gast, Chenfanfu Jiang, and Joseph Teran. 2017. A polynomial particle-in-cell method. *ACM Transactions on Graphics (TOG)* 36, 6 (2017), 1–12.
- Ming Gao, Andre Pradhana, Xuchen Han, Qi Guo, Grant Kot, Eftychios Sifakis, and Chenfanfu Jiang. 2018. Animating fluid sediment mixture in particle-laden flows. *ACM Transactions on Graphics (TOG)* 37, 4 (2018), 1–11.
- Christoph Gissler, Andreas Henne, Stefan Band, Andreas Peer, and Matthias Teschner. 2020. An implicit compressible SPH solver for snow simulation. *ACM Transactions on Graphics (TOG)* 39, 4 (2020), 36–1.
- Christoph Gissler, Andreas Peer, Stefan Band, Jan Bender, and Matthias Teschner. 2019. Interlinked SPH pressure solvers for strong fluid-rigid coupling. *ACM Transactions on Graphics (TOG)* 38, 1 (2019), 1–13.
- Prashant Goswami and Christopher Batty. 2014. Regional Time Stepping for SPH. In *Eurographics 2014 - Short Papers*, Eric Galin and Michael Wand (Eds.). The Eurographics Association. <https://doi.org/10.2312/egsh.20141011>
- Simon Green. 2010. Particle simulation using cuda. *NVIDIA whitepaper* 6 (2010), 121–128.
- Kensuke Harasaki and Mitsuteru Asai. 2016. Fluid-soil multiphase flow simulation by an SPH-DEM coupled method. In *The 2016 World Congress on Advances in Civil, Environmental, and Materials Research (ACEM16), Jeju Island, Korea, August 28-September*, Vol. 1.
- Sébastien Hentz, Frédéric V Donzé, and Laurent Daudeville. 2004. Discrete element modelling of concrete submitted to dynamic loading at high strain rates. *Computers & structures* 82, 29-30 (2004), 2509–2524.
- Yuanming Hu, Yu Fang, Ziheng Ge, Ziyin Qu, Yixin Zhu, Andre Pradhana, and Chenfanfu Jiang. 2018. A moving least squares material point method with displacement discontinuity and two-way rigid body coupling. *ACM Transactions on Graphics (TOG)* 37, 4 (2018), 1–14.
- Libo Huang, Torsten Hädrich, and Dominik L Michels. 2019. On the accurate large-scale simulation of ferrofluids. *ACM Transactions on Graphics (TOG)* 38, 4 (2019), 1–15.
- Markus Ihmsen, Jens Cornelis, Barbara Solenthaler, Christopher Horvath, and Matthias Teschner. 2013. Implicit incompressible SPH. *IEEE transactions on visualization and computer graphics* 20, 3 (2013), 426–435.
- Jacob N. Israelachvili. 2011. 17 - Adhesion and Wetting Phenomena. In *Intermolecular and Surface Forces (Third Edition)* (third edition ed.), Jacob N. Israelachvili (Ed.). Academic Press, San Diego, 415–467. <https://doi.org/10.1016/B978-0-12-375182-9.10017-X>
- Chenfanfu Jiang, Theodore Gast, and Joseph Teran. 2017. Anisotropic elastoplasticity for cloth, knit and hair frictional contact. *ACM Transactions on Graphics (TOG)* 36, 4 (2017), 1–14.
- Chenfanfu Jiang, Craig Schroeder, Andrew Selle, Joseph Teran, and Alexey Stomakhin. 2015. The affine particle-in-cell method. *ACM Transactions on Graphics (TOG)* 34, 4 (2015), 1–10.
- Chenfanfu Jiang, Craig Schroeder, Joseph Teran, Alexey Stomakhin, and Andrew Selle. 2016. The material point method for simulating continuum materials. In *ACM SIGGRAPH 2016 Courses*. 1–52.
- Y Jiang, C Li, S Deng, and SM Hu. 2020. A Divergence-free Mixture Model for Multiphase Fluids. In *Computer Graphics Forum*, Vol. 39. Wiley Online Library, 69–77.
- Victor Kaliakin. 2017. *Soil Mechanics: Calculations, Principles, and Methods*. Butterworth-Heinemann.
- Richard Keiser, Bart Adams, Dominique Gasser, Paolo Bazzi, Philip Dutré, and Markus Gross. 2005. A unified lagrangian approach to solid-fluid animation. In *Proceedings Eurographics/IEEE VGTC Symposium Point-Based Graphics, 2005*. IEEE, 125–148.
- Dan Koschier, Jan Bender, Barbara Solenthaler, and Matthias Teschner. 2020. Smoothed particle hydrodynamics techniques for the physics based simulation of fluids and solids. *arXiv preprint arXiv:2009.06944* (2020).
- Toon Lenaerts, Bart Adams, and Philip Dutré. 2008. Porous flow in particle-based fluid simulations. *ACM Transactions on Graphics (TOG)* 27, 3 (2008), 1–8.
- Toon Lenaerts and Philip Dutré. 2009. Mixing fluids and granular materials. In *Computer Graphics Forum (Proceedings of Eurographics 2009)*, Vol. 28. 213–218. <https://doi.org/10.1111/j.1467-8659.2009.01360.x>
- Juoping Lian, Colin Thornton, and Michael J. Adams. 1993. A Theoretical Study of the Liquid Bridge Forces between Two Rigid Spherical Bodies. *Journal of Colloid and Interface Science* 161, 1 (1993), 138–147. <https://doi.org/10.1006/jcis.1993.1452>

- Leon B Lucy. 1977. A numerical approach to the testing of the fission hypothesis. *The astronomical journal* 82 (1977), 1013–1024.
- Joe J Monaghan. 1992. Smoothed particle hydrodynamics. *Annual review of astronomy and astrophysics* 30, 1 (1992), 543–574.
- Matthias Müller, Barbara Solenthaler, Richard Keiser, and Markus Gross. 2005. Particle-based fluid-fluid interaction. In *Proceedings of the 2005 ACM SIGGRAPH/Eurographics symposium on Computer animation*. 237–244.
- Michael B Nielsen and Ole Østerby. 2013. A two-continua approach to Eulerian simulation of water spray. *ACM Transactions on Graphics (TOG)* 32, 4 (2013), 1–10.
- Andreas Peer, Christoph Gissler, Stefan Band, and Matthias Teschner. 2018. An implicit SPH formulation for incompressible linearly elastic solids. In *Computer Graphics Forum*, Vol. 37. Wiley Online Library, 135–148.
- Andreas Peer, Markus Ihmsen, Jens Cornelis, and Matthias Teschner. 2015. An implicit viscosity formulation for SPH fluids. *ACM Transactions on Graphics (TOG)* 34, 4 (2015), 1–10.
- Daniel J Price. 2012. Smoothed particle hydrodynamics and magnetohydrodynamics. *J. Comput. Phys.* 231, 3 (2012), 759–794.
- Yakov I Rabinovich, Madhavan S Esayanur, and Brij M Moudgil. 2005. Capillary forces between two spheres with a fixed volume liquid bridge: theory and experiment. *Langmuir* 21, 24 (2005), 10992–10997.
- Bo Ren, Chenfeng Li, Xiao Yan, Ming C Lin, Javier Bonet, and Shi-Min Hu. 2014. Multiple-fluid SPH simulation using a mixture model. *ACM Transactions on Graphics (TOG)* 33, 5 (2014), 1–11.
- Bo Ren, Xu-Yun Yang, Ming C Lin, Nils Thuerey, Matthias Teschner, and Chenfeng Li. 2018. Visual simulation of multiple fluids in computer graphics: A state-of-the-art report. *Journal of Computer Science and Technology* 33, 3 (2018), 431–451.
- Witawat Rungjirathananon, Zoltan Szego, Yoshihiro Kanamori, and Tomoyuki Nishita. 2008. Real-time animation of sand-water interaction. In *Computer Graphics Forum*, Vol. 27. Wiley Online Library, 1887–1893.
- Barbara Solenthaler and Renato Pajarola. 2009. Predictive-corrective incompressible SPH. In *ACM SIGGRAPH 2009 papers*. 1–6.
- Barbara Solenthaler, Jürg Schläfli, and Renato Pajarola. 2007. A unified particle model for fluid–solid interactions. *Computer Animation and Virtual Worlds* 18, 1 (2007), 69–82.
- Deborah Sulsky, Shi-Jian Zhou, and Howard L Schreyer. 1995. Application of a particle-in-cell method to solid mechanics. *Computer physics communications* 87, 1-2 (1995), 236–252.
- Xiaosong Sun, Mikio Sakai, and Yoshinori Yamada. 2013. Three-dimensional simulation of a solid–liquid flow by the DEM–SPH method. *J. Comput. Phys.* 248 (2013), 147–176.
- Andre Pradhana Tampubolon, Theodore Gast, Gergely Klár, Chuyuan Fu, Joseph Teran, Chenfanfu Jiang, and Ken Museth. 2017. Multi-species simulation of porous sand and water mixtures. *ACM Transactions on Graphics (TOG)* 36, 4 (2017), 1–11.
- Hai Tan and Shenghong Chen. 2017. A hybrid DEM-SPH model for deformable landslide and its generated surge waves. *Advances in Water Resources* 108 (2017), 256–276.
- Federico A Tavarez and Michael E Plesha. 2007. Discrete element method for modelling solid and particulate materials. *International journal for numerical methods in engineering* 70, 4 (2007), 379–404.
- Christopher D Willett, Michael J Adams, Simon A Johnson, and Jonathan PK Seville. 2000. Capillary bridges between two spherical bodies. *Langmuir* 16, 24 (2000), 9396–9405.
- Qiong Xiao and Ji-Peng Wang. 2020. CFD–DEM simulations of seepage-induced erosion. *Water* 12, 3 (2020), 678.
- Wen-Jie Xu, Xue-Yang Dong, and Wen-Tao Ding. 2019. Analysis of fluid-particle interaction in granular materials using coupled SPH-DEM method. *Powder Technology* 353 (2019), 459–472. <https://doi.org/10.1016/j.powtec.2019.05.052>
- Xiao Yan, Yun-Tao Jiang, Chen-Feng Li, Ralph R Martin, and Shi-Min Hu. 2016. Multiphase SPH simulation for interactive fluids and solids. *ACM Transactions on Graphics (TOG)* 35, 4 (2016), 1–11.
- Xiao Yan, C-F Li, X-S Chen, and S-M Hu. 2018. MPM simulation of interacting fluids and solids. In *Computer Graphics Forum*, Vol. 37. Wiley Online Library, 183–193.
- Tao Yang, Jian Chang, Ming C Lin, Ralph R Martin, Jian J Zhang, and Shi-Min Hu. 2017. A unified particle system framework for multi-phase, multi-material visual simulations. *ACM Transactions on Graphics (TOG)* 36, 6 (2017), 1–13.
- Tao Yang, Jian Chang, Bo Ren, Ming C Lin, Jian Jun Zhang, and Shi-Min Hu. 2015. Fast multiple-fluid simulation using Helmholtz free energy. *ACM Transactions on Graphics (TOG)* 34, 6 (2015), 1–11.
- Siti Aimi Nadia Mohd Yusoff, Ismail Bakar, DC Wijeyesekera, Adnan Zainorabidin, Mastura Azmi, and Harris Ramli. 2017. The effects of different compaction energy on geotechnical properties of kaolin and laterite. In *AIP Conference Proceedings*, Vol. 1875. AIP Publishing LLC, 030009.
- Wenqi Zhong, Aibing Yu, Xuejiao Liu, Zhenbo Tong, and Hao Zhang. 2016. DEM/CFD-DEM modelling of non-spherical particulate systems: theoretical developments and applications. *Powder Technology* 302 (2016), 108–152.
- ZY Zhou, SB Kuang, KW Chu, and AB Yu. 2010. Discrete particle simulation of particle-fluid flow: model formulations and their applicability. *Journal of Fluid Mechanics* 661 (2010), 482.